Journal of Alloys and Compounds, 191 (1993) 255–261
JALCOM 523

Production of amorphous bulk materials of an $Nd_{15}Fe_{77}B_8$ magnetic alloy and their magnetic properties

T. Harada and T. Kuji
Corporate R & D Centre, Mitsui Mining & Smelting Co. Ltd., 1333-2 Haraichi, Ageo, Saitama 362 (Japan)

K. Fukuoka and Y. Syono
Institute for Materials Research, Tohoku University, Katahira, Sendai 980 (Japan)

(Received August 31, 1992)

Abstract

Amorphous bulk $Nd_{15}Fe_{77}B_8$ materials were produced by dynamic compaction of the amorphous powders. X-ray diffraction and differential scanning calorimetry studies confirmed that the amorphous structure was well maintained in the compacted materials. No appreciable crystallites were seen in the microstructures of the compacted materials. Only at the particle boundary was there some melting during dynamic compaction, with the result that a small fraction of fine $Nd_2Fe_{14}B$ crystallites was found in the microstructure. The amorphous bulk materials showed low coercivity values as expected for amorphous Nd–Fe–B materials. Heat treatment of the bulk amorphous materials yielded changes in the physical and mechanical properties due to the $Nd_2Fe_{14}B$ precipitates. Heat treatment just above the crystallization temperature resulted in the formation of very fine precipitates (0.1 μm) of the $Nd_2Fe_{14}B$ ferromagnetic phase, giving rise to high coercivity and high microhardness values. The annealed materials were magnetically isotropic and showed a maximum energy product of 80 kJ m^{-3}.

1. Introduction

It is known that sufficiently high solidification rates result in the formation of amorphous structures. Rapid solidification processing (RSP) techniques, such as melt spinning and gas atomization, give amorphous materials in splat, wire, ribbon, sheet or powder form [1–5]. The maximum thickness of the amorphous materials is typically less than a few hundredths of a millimetre so as to accomplish high solidification rates. Alternatively, amorphous materials can be obtained by mechanical alloying (MA) [6]. However, MA gives amorphous materials in the powder form. The shapes of the amorphous materials severely restrict their application even though they have many advantages, *i.e.* high mechanical strength, good ductility, good magnetic properties, high corrosion resistance, etc. Therefore there is the need for the production of new processing techniques to obtain bulk amorphous materials. Such bulk amorphous materials may be useful as soft magnetic cores, shields, inductors, rotors, tape heads, etc. In addition, the heat treatment of bulk amorphous materials creates a variety of mechanical and hard or soft magnetic applications, reflecting the microcrystalline structures.

Conventionally, powders and ribbons produced by RSP are consolidated into bulk form using powder metallurgy techniques. The most common techniques used for consolidation are hot isostatic pressing, hot pressing and hot extrusion [7]. However, these techniques may decrease, modify or eliminate useful properties because such heat exposure generally results in the precipitation of crystallites, with a totally different combination of properties. If the amorphous structure has to be retained, the consolidation parameters such as temperature, time and pressure must be controlled very carefully [8]. In particular, lower consolidation temperatures are preferred to avoid crystallization. Amorphous materials, therefore, have usually been consolidated by cold compaction methods, such as cold isostatic pressing, hydrostatic extrusion, forging, rolling and dynamic compaction [7]. Because of the high strength of these materials and the necessity of preserving the amorphous structure, dynamic compaction is preferred.

There have been several attempts to consolidate amorphous powders or ribbons into bulk materials by dynamic compaction [9, 10]. In this study, we have chosen to investigate Nd–Fe–B alloys, which have attracted growing interest as high performance permanent magnets [11–13]. We have recently reported that amorphous Nd–Fe–B powders can be successfully consolidated into bulk form without losing their amorphous

0925-8388/93/$6.00

structure by dynamic compaction [14]. This work is an attempt to clarify the microstructure and magnetic properties of the amorphous bulk $Nd_{15}Fe_{77}B_8$ materials and to investigate the effect of annealing on the magnetic and mechanical properties of these materials.

2. Experimental details

$Nd_{15}Fe_{77}B_8$ alloy was prepared by arc melting in an argon atmosphere. The alloy (20 g) was induction melted and superheated to about 1623 K under an argon atmosphere in a quartz crucible having an orifice (diameter, 0.6 mm) at the bottom. The molten metal was ejected through the orifice with argon onto a chromium-plated copper wheel (diameter, 30 cm) rotating at a surface velocity of 52 m s^{-1}. The resultant melt-spun ribbons were obtained as fragmented pieces (thickness, 20 μm; width, 2 mm). The melt-spun ribbons were brittle and could be comminuted mechanically and subsequently sieved to give particle sizes in the range 40–210 μm. The powders were placed in a steel container (SCM3), and dynamically compacted by the impact of an aluminium flyer launched by a 25 mm propellant gun. The gun facilities and process have been described in detail elsewhere [15]. The shock pressure in the container was calculated to be 20 GPa by the impedance-matching technique and the Hugoniots of the materials involved in the collision before dynamic compaction; this led to an optimal density of bulk amorphous materials in our previous study [14].

The samples were taken out of the container after dynamic compaction. They had been successfully consolidated into bulk materials. Typical dimensions of the compacted materials were 13 mm thick and 25 mm in diameter. The density of the compacted materials, measured by Archimedes' method, was 7.0 Mg m^{-3} (approximately 93% of the ingot density). Specimens were cut from these compacted materials for further processing and property measurements. Heat treatments were performed in an argon atmosphere at temperatures between 773 and 1173 K for 1.8 ks. After the heat treatment, the specimens were quenched from the annealing temperature. The amorphous state of the compacted materials was confirmed by X-ray diffraction (XRD) using Cu Kα radiation. The crystallization behaviour of the compacted materials was measured in an argon atmosphere at a heating rate of 0.33 K s^{-1} using differential scanning calorimetry (DSC). The microstructures of the compacted materials were investigated using scanning electron microscopy (SEM) and transmission electron microscopy (TEM). Thin foil specimens for TEM studies were prepared by combining mechanical and ion beam thinnings. The mechanical properties of the specimens were examined at room temperature using a microhardness tester with a Vickers-type diamond pyramid indenter at a load of 0.2 N. The magnetic properties of the samples were measured at room temperature by a recording fluxmeter using an electromagnet with a maximum applied field of 1.9 MA m^{-1}.

3. Results and discussion

3.1. As-compacted materials

In the Nd–Fe–B ternary system, only the $Nd_2Fe_{14}B$ phase has both a large saturation magnetization and a high anisotropy field, which are essential for use as a permanent magnet. Nd–Fe–B magnets generally have the off-stoichiometric composition $Nd_2Fe_{14}B$. One of the typical compositions, which has been widely studied and produced, is $Nd_{15}Fe_{77}B_8$ [11, 16, 17]. Figure 1 shows the results of XRD studies of the ingots, the melt-spun ribbons and the compacted materials. According to the phase diagram, the $Nd_{15}Fe_{77}B_8$ alloy should pertain to a three-phase region which consists of $Nd_2Fe_{14}B$, Nd and $Nd_{1.1}Fe_4B_4$ phases [18]. The XRD pattern of the ingots is well indexed according to the tetragonal $Nd_2Fe_{14}B$ phase. However, no clear diffraction peaks are found from the other phases because of the large fraction of the $Nd_2Fe_{14}B$ phase in the $Nd_{15}Fe_{77}B_8$ alloy. The XRD patterns of the melt-spun ribbons and the compacted materials show no indication of these peaks, but exhibit a broad maximum at around 40°. Such broad halos are characteristic of amorphous structures. This suggests that the compacted materials and the melt-spun ribbons are essentially in the amorphous state.

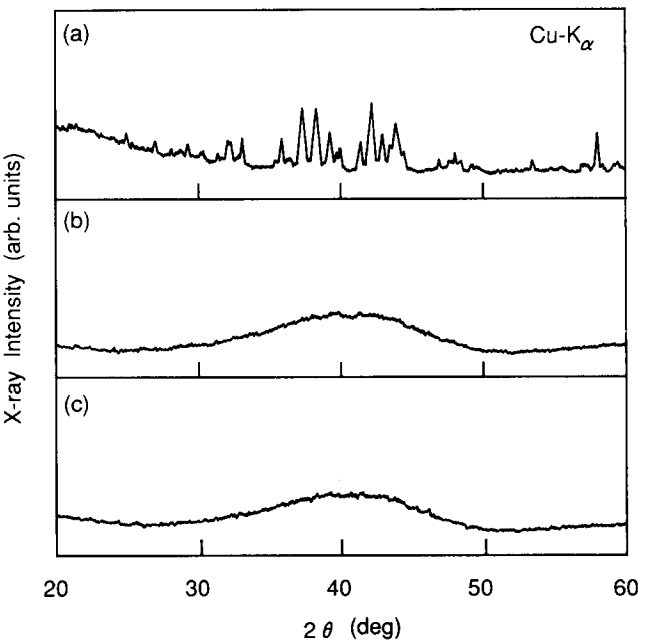

Fig. 1. XRD patterns of $Nd_{15}Fe_{77}B_8$ alloy: (a) ingots; (b) melt-spun ribbons; (c) compacted materials.

Figure 2 shows the DSC curve of the compacted materials measured at a heating rate of 0.33 K s^{-1} in an argon atmosphere. DSC studies for the compacted materials show an exothermic peak at around 870 K due to the transformation of amorphous to crystalline states. The crystallization enthalpy of the compacted materials is 3.7 kJ mol^{-1}. This value agrees well with that of amorphous melt-spun ribbons with the same composition [19]. This also confirms that the compacted materials have an amorphous structure. After the DSC measurements, XRD studies were performed to examine the crystalline phase. It was found that the specimens consisted of tetragonal $Nd_2Fe_{14}B$ phase. Thus the exothermic peak at about 870 K is due to the crystallization of the $Nd_2Fe_{14}B$ phase from the amorphous material.

Figure 3 shows transmission electron micrographs and a corresponding scanning electron micrograph of the compacted materials. Although some small cavities are seen, the microstructure of the compacted materials is featureless and no particle boundary is seen in the scanning electron micrograph. In dynamic compaction, the shock wave produced by the impact of the projectile compacts the powders. Heat generated by closing of the gap between the particles melts the particle surface and the melt bonds the particles together. The heat generated by dynamic compaction may affect the amorphous matrix and cause the precipitation of crystalline material. However, no precipitates were observed in the microstructure of the compacted material by SEM studies. Several thin-sliced specimens were prepared and further microstructural studies were performed by TEM. Figure 3(b) shows a typical microstructure of the compacted materials. The microstructure of the

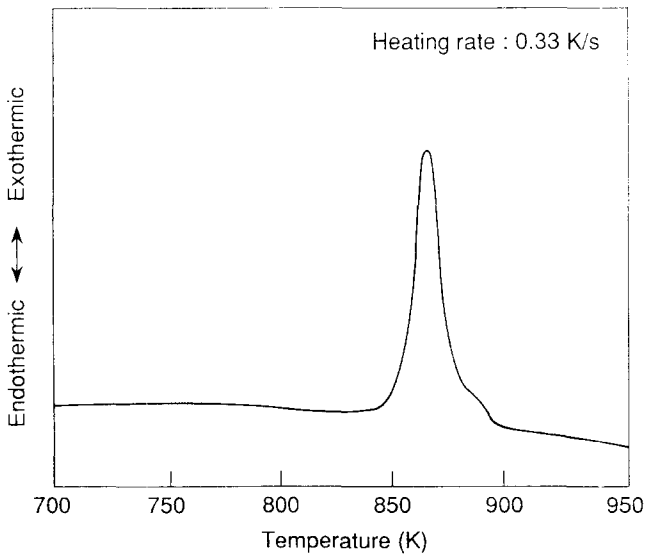

Fig. 2. DSC curve of compacted materials measured at a heating rate of 0.33 K s^{-1} in an argon atmosphere.

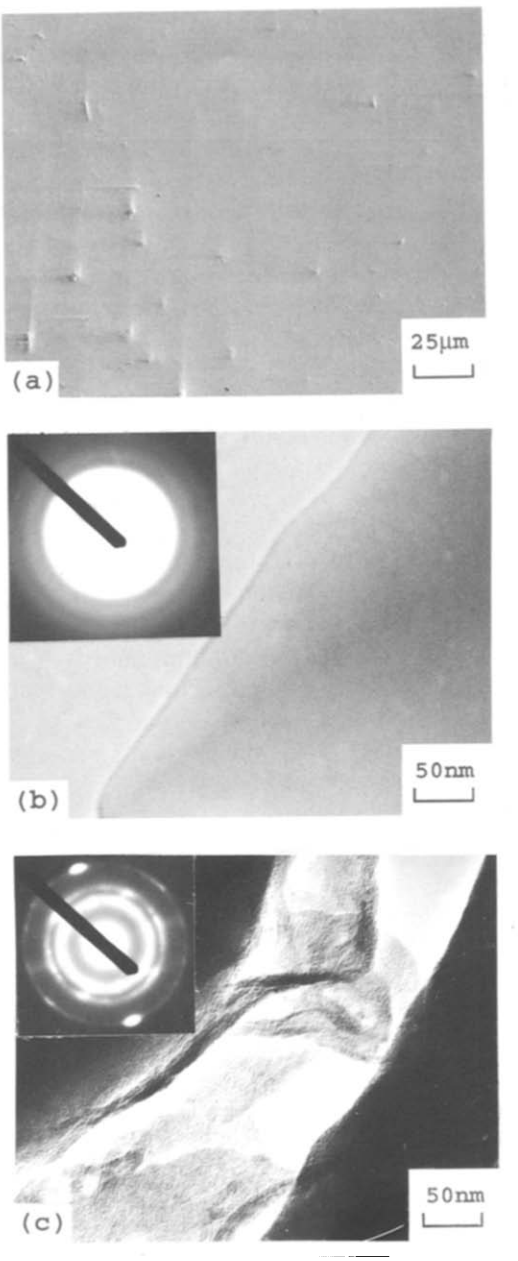

Fig. 3. Transmission electron and scanning electron micrographs of compacted materials: (a) scanning electron micrograph; (b) transmission electron micrograph and a corresponding SAD pattern of the matrix; (c) transmission electron micrograph and a corresponding SAD pattern of the particle boundary.

compacted material is featureless as is the scanning electron micrograph. The corresponding selected area diffraction (SAD) pattern of the specimen shows a broad so-called "halo" pattern, which is characteristic of amorphous materials. This also confirms that the compacted materials have an amorphous structure.

Crystallite phases in layers within the amorphous matrix can be seen in the transmission electron micrograph shown in Fig. 3(c). This crystalline layer is supposed to be the particle boundary where the surface

of the particle melted and solidified during dynamic compaction. With the exception of the rings with small diameters, the rings in the SAD pattern fitted well with the calculated d spacings using the lattice parameters of the $Nd_2Fe_{14}B$ phase. This suggests that the particle boundary consists of the fine $Nd_2Fe_{14}B$ phase and amorphous materials. The thickness of the boundary is about 0.1 μm. Compared with the thickness of the amorphous powders (20 μm), the volume of the melt is less than 1% of the whole particle. This indicates that only a small portion of the particle surface is melted by the heat generated during dynamic compaction, and the melt solidifies and bonds the particles together. Although small amounts of crystallites exist along the particle boundaries in the compacted materials, most of the particle retains an amorphous structure.

Dynamic compaction of the amorphous powders at a shock pressure of 20 GPa melts only a small fraction of the particle surface and the heat generated by dynamic compaction does not affect the amorphous matrix. Thus it may be possible to produce a perfect bulk amorphous material. Under the condition that only a very small fraction of the particle melts, the melt may solidify rapidly and this will result in complete formation of bulk amorphous material. Such a perfect bulk amorphous material may be obtained by optimizing the conditions for dynamic compaction.

Figure 4 shows a hysteresis curve of the compacted material. It has been reported that amorphization in Nd–Fe–B melt-spun ribbons decreases the coercivity and the amorphous melt-spun ribbons show low coercivity values [12, 20]. In this work, the coercivity of the amorphous melt-spun ribbons is typically less than 8 kA m^{-1}. The coercivity of the compacted material remains as low as that of the amorphous melt-spun ribbons. This suggests that the compacted materials are amorphous. However, the shape of the hysteresis loop of the bulk amorphous material is slightly different from that of the amorphous melt-spun ribbons. Similar hysteresis loops are often observed when amorphous materials coexist with the ferromagnetic $Nd_2Fe_{14}B$ phase in Nd–Fe–B melt-spun ribbons [21]. Thus the compacted materials contain mainly amorphous phase, but also a small fraction of a hard magnetic phase such as $Nd_2Fe_{14}B$ crystallites. This is consistent with the results of TEM studies which demonstrate the existence of the ferromagnetic $Nd_2Fe_{14}B$ phase at particle boundaries. The compacted materials contain about 0.24 wt.% oxygen. This suggests that the change in the hysteresis loop may be partially due to contamination by oxides. The effect of the residual strain from the shock pressure may also affect the shape of the hysteresis loop [22].

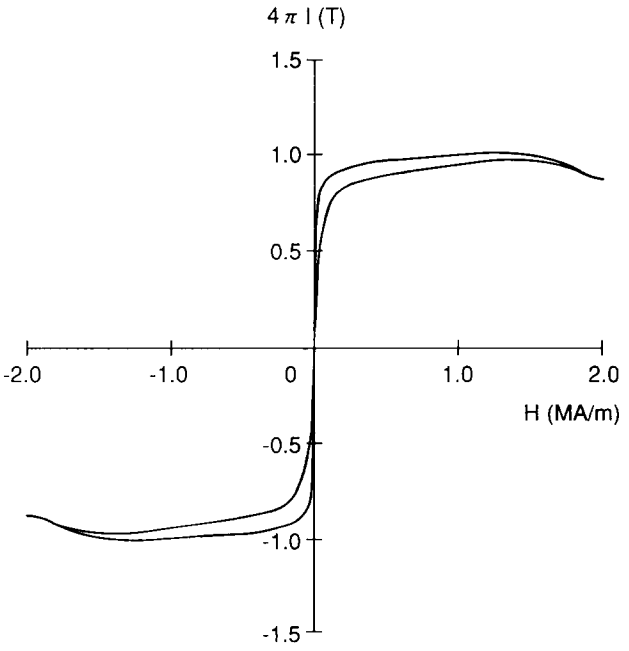

Fig. 4. Hysteresis curve of compacted material.

3.2. Heat-treated materials

In amorphous materials, heating above the crystallization temperature results in the precipitation of crystallites. In the compacted $Nd_{15}Fe_{77}B_8$ materials, the crystallization temperature of the $Nd_2Fe_{77}B$ phase from the amorphous state, determined by DSC measurements, is around 870 K. The crystallization temperature varies with time and temperature during isochronal annealing [23]. Therefore isothermal annealing was carried out to modify the structure around the crystallization temperature. Figure 5 shows the XRD patterns of the compacted materials annealed at temperatures between 773 and 1173 K for 1.8 ks, together with the XRD pattern of the as-compacted materials. Virtually no indication of crystallinity is found for the sample annealed at 773 K. However, the XRD pattern does not show a broad maximum, which is characteristic of amorphous materials. DSC studies of the annealed sample show an exothermic peak at around 870 K as is the case for the original amorphous materials. Therefore the sample annealed at 773 K retains an amorphous structure. Small diffraction peaks are observed in the samples annealed above 873 K. The small diffraction peaks of the samples match those of $Nd_2Fe_{14}B$. DSC studies of the sample annealed at 873 K do not show any exothermic peak as expected for the crystalline materials. Thus the samples annealed above 873 K do not have an amorphous structure but consist of the $Nd_2Fe_{14}B$ phase. The XRD peaks of the $Nd_2Fe_{14}B$ phase for the annealed samples become sharper as the annealing temperature increases. This indicates that the grain size increases as the annealing temperature increases.

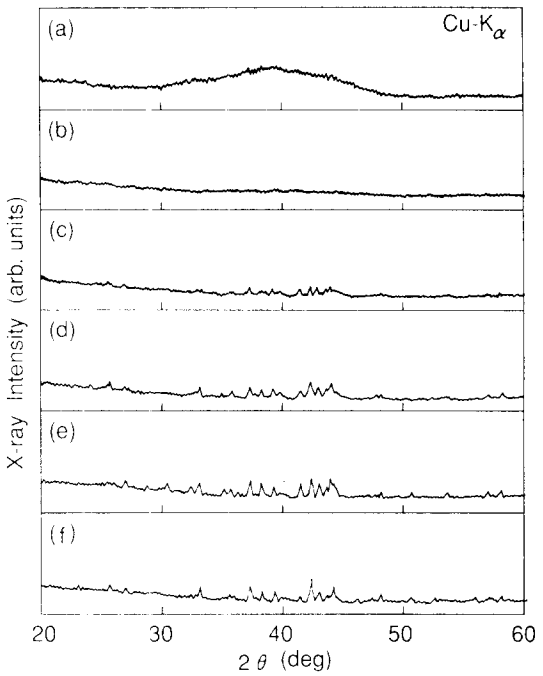

Fig. 5. XRD patterns of as-compacted materials (a) and materials annealed at 773 K (b), 873 K (c), 973 K (d), 1073 K (e) and 1173 K (f) for 1.8 ks.

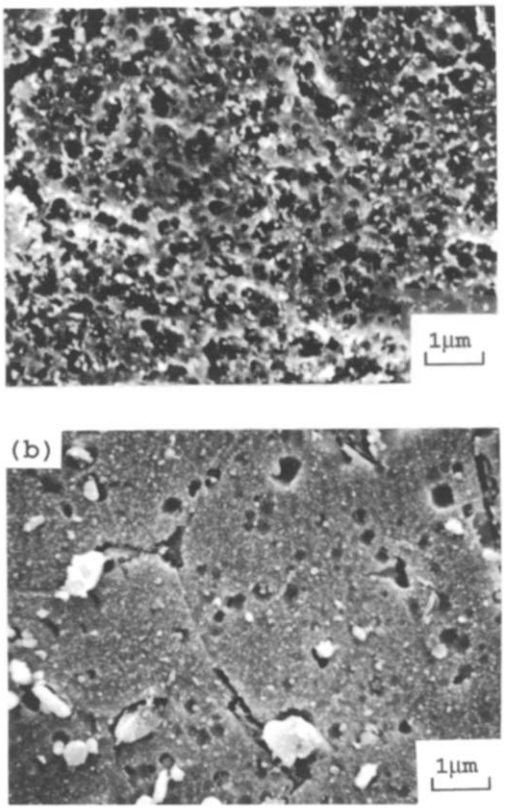

Fig. 6. Scanning electron micrographs of the compacted materials annealed at 873 K (a) and 1173 K (b) for 1.8 ks.

Figure 6 shows scanning electron micrographs of the compacted materials annealed at 873 K (a) and 1173 K (b). The compacted materials have an amorphous structure and hence show a featureless microstructure. When the compacted materials are annealed at 873 K, very fine precipitates are observed in the scanning electron micrograph. A TEM study of the sample annealed at 873 K reveals that the fine precipitates are $Nd_2Fe_{14}B$ and that the average crystallite size is about 0.1 μm. The single domain size of the $Nd_2Fe_{14}B$ phase is estimated to be 0.3 μm [24]. The $Nd_2Fe_{14}B$ grains in the sample annealed at 873 K are probably single domain particles. Virtually the same scanning electron micrographs are obtained for the samples annealed at 973 and 1073 K. However, relatively large precipitates (about 3 μm) are observed for the sample annealed at 1173 K. These results indicate that grain growth of the $Nd_2Fe_{14}B$ phase is significant at 1173 K, but is suppressed during annealing below 1073 K. The boundary phase for the sample annealed at 873 K was not determined by energy dispersive X-ray (EDX) analysis. However, the grain boundary for the sample annealed at 1173 K was determined to be the Nd phase as expected for the $Nd_{15}Fe_{77}B_8$ alloy.

Figure 7 shows the dependence of the intrinsic coercivity $_iH_c$ on the annealing temperature for the compacted materials. The materials initially have an amorphous structure and hence show very low coercivity values. The coercivity of the materials, when annealed at 773 K, remains as low as that of the as-compacted material, but increases rapidly on annealing at 873 K. The highest coercivity of 1.27 MA m^{-1} is obtained for samples annealed at 873 K. The coercivity decreases

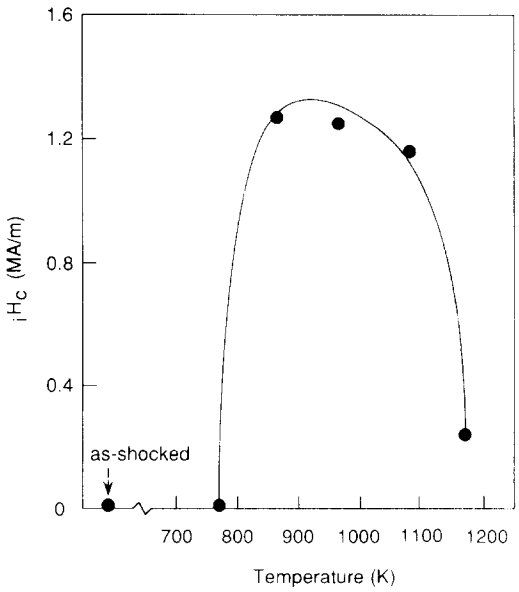

Fig. 7. Dependence of the intrinsic coercivity $_iH_c$ on the annealing temperature for the compacted materials.

gradually between 873 and 1073 K and then decreases rapidly above 1073 K. According to the XRD and SEM studies, the observed rapid increase in ${}_iH_c$ at 873 K is caused by the formation of $Nd_2Fe_{14}B$ crystallites. When the compacted materials are annealed at temperatures between 873 and 1073 K, the $Nd_2Fe_{14}B$ grains remain small and show attractively high coercivity values. However, when the $Nd_2Fe_{14}B$ crystallites become much larger than the single domain size, the compacted materials show lower coercivity values. This is consistent with the results obtained by the heat treatment of amorphous Nd–Fe–B materials [25, 26].

Figure 8 shows the demagnetization curves of the compacted materials (as compacted (a) and after annealing at 873 K for 1.8 ks (b)). Specimens cut from the compacted materials were measured in directions both parallel and normal to the direction of dynamic compaction. Virtually the same hysteresis loops are obtained in both directions. The annealed materials are magnetically isotropic as is the case for melt-spun ribbons, indicating that the $Nd_2Fe_{14}B$ crystallites precipitate in random orientations during annealing. The maximum energy product and the intrinsic coercivity values increase sharply to 80 kJ m^{-3} and 1.27 MA m^{-1} respectively on annealing as shown in Fig. 8(b).

The mechanical properties of Nd–Fe–B magnetic materials are important in the fabrication of magnets and for the evaluation of the effects of processing variables. Microhardness measurements have been used to measure the mechanical properties of numerous alloys and have received wide acceptance in research work on materials [27]. Figure 9 shows the dependence of the microhardness value H_V on the annealing temperature (773–1173 K) for the compacted materials. The accuracy of the microhardness values depends on the applied load. In the experiments, an applied load

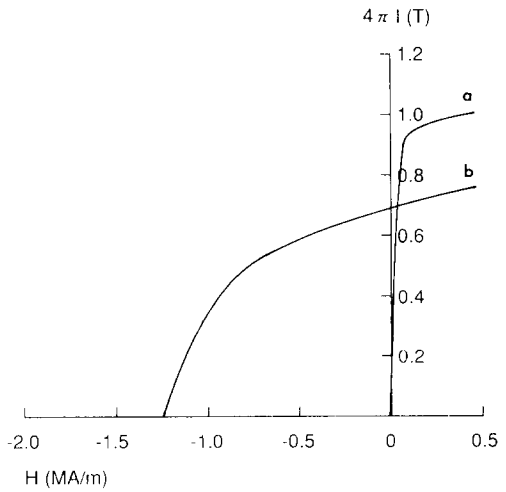

Fig. 8. Demagnetization curves of compacted materials: as-compacted (a) and after annealing at 873 K for 1.8 ks (b).

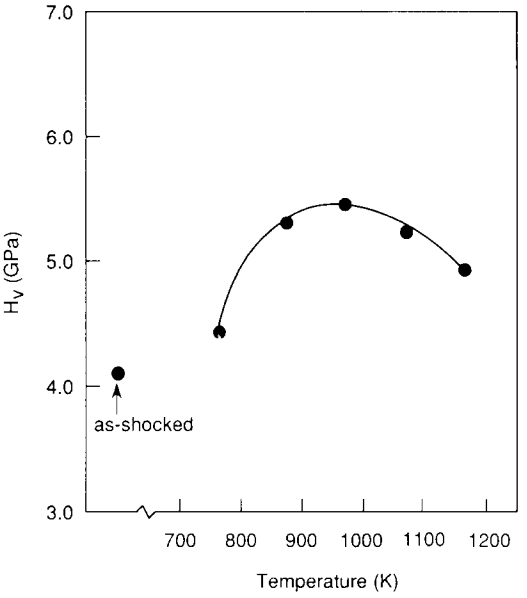

Fig. 9. Dependence of the microhardness value H_V on the annealing temperature for the compacted materials.

of 0.2 N was selected for the measurements. The microhardness value of the specimen annealed at 773 K is slightly larger than that of the bulk amorphous material. This suggests that the mechanical properties of the compacted materials change during annealing at 773 K. The microhardness value increases and reaches a plateau between 873 and 973 K as the annealing temperature increases. It then decreases as the annealing temperature increases. The maximum microhardness value, $H_V = 5.4$ GPa, is obtained at 973 K. This suggests that the microhardness values reach a maximum when fine precipitates of the $Nd_2Fe_{14}B$ phase are obtained. As the $Nd_2Fe_{14}B$ grains become larger, the microhardness value decreases. This indicates that the microhardness depends on the size of the $Nd_2Fe_{14}B$ phase as is the case for the coercivity. According to the results of both XRD and DSC analyses, the sample annealed at 773 K retains an amorphous structure. However, the microhardness measurement suggests that the mechanical properties of the compacted materials change. A slight increase in structural relaxation during heat treatment results in an increase in the microhardness value, suggesting that microhardness measurements are very sensitive to structural changes.

Heat treatment of the amorphous bulk materials above the crystallization temperature results in the precipitation of the $Nd_2Fe_{14}B$ phase. With continued heating at temperatures above the crystallization temperature, the fine grains grow larger and, as a result, yield changes in the magnetic and mechanical properties. Both the coercivity and microhardness values strongly depend on the annealing temperature, *i.e.* the crystallite

size of the $Nd_2Fe_{14}B$ grains. The fine precipitates of the $Nd_2Fe_{14}B$ phase give rise to both high coercivity and high microhardness values. Large $Nd_2Fe_{14}B$ grains lead to a decrease in the coercivity of the Nd–Fe–B alloys as they are deleterious to the mechanical behaviour of metals and alloys.

4. Conclusions

Amorphous $Nd_{15}Fe_{77}B_8$ melt-spun ribbons have been consolidated by dynamic compaction using the gun method. The compacted materials were identified to be amorphous by XRD and electron diffraction. DSC measurements confirmed the existence of the amorphous materials, and the crystallization enthalpy of the compacted materials was comparable with that of the amorphous melt-spun ribbons. The microstructures of the compacted materials were featureless as expected for amorphous materials. However, very fine $Nd_2Fe_{14}B$ crystallites were found in particle boundaries by detailed TEM studies. These results indicate that heat generated by dynamic compaction melts only a small fraction of the particle surface and the particle itself remains in the amorphous state. The compacted materials consist mainly of an amorphous structure and show a low coercivity.

Heat treatment of the amorphous bulk materials at 873 K caused the formation of $Nd_2Fe_{14}B$ crystallites. The grain growth of the $Nd_2Fe_{14}B$ crystallites was quite limited at temperatures below 1073 K, but was significant at 1173 K. When the microstructures consisted of fine $Nd_2Fe_{14}B$ precipitates (around 0.1 μm), the annealed materials showed a maximum coercivity of 1.27 MA m^{-1}. The annealed materials were magnetically isotropic and showed a maximum energy product of 80 kJ m^{-3}. The microhardness value of the specimen annealed at 773 K was slightly larger than that of the bulk amorphous material. The microhardness value increased and reached a plateau between 873 and 973 K, and then decreased as the annealing temperature increased. The maximum microhardness value, $H_V = 5.4$ GPa, was obtained at 973 K. Both the coercivity and microhardness values were strongly related to the size of the $Nd_2Fe_{14}B$ crystallites.

Acknowledgments

This work was conducted in the programme, Advanced Chemical Processing Technology, consigned to the Advanced Chemical Processing Technology Research Association from the New Energy and Industrial Technology Development Organization, which was carried out under the Large-Scale Project enforced by the Agency of Industrial Science and Technology, Ministry of International Trade and Industry. The authors are grateful to Ms. N. Hanzawa for the TEM analysis.

References

1 P. Duwez and R. H. Willens, *Trans. Metall. Soc. AIME, 227* (1963) 362.
2 T. Masumoto, I. Ohnaka, A. Inoue and M. Hagiwara, *Scr. Metall., 15* (1981) 293.
3 R. Pond and R. Maddin, *Trans. Metall. Soc. AIME, 245* (1969) 407.
4 R. E. Maringer and C. E. Mobley, *J. Vac. Sci. Technol., 11* (1974) 1067.
5 N. J. Grant, in R. Mehrabian, B. H. Kear and M. Cohen (eds.), *Rapid Solidification Processing, Principles and Technologies,* Claitor's Publishing Division, Baton Rouge, LA, 1977, p. 230.
6 E. Hellstern and L. Schultz, *Appl. Phys. Lett., 48* (1986) 124.
7 T. R. Anantheraman and C. Suryanarayana, *Key Eng. Mater., 17* (1987) 1.
8 P. H. Shingu, *Mater. Sci. Eng., 97* (1988) 137.
9 R. Hasegawa and C. F. Cline, in S. Steeb and H. Warlimont (eds.), *Proc. 5th Int. Conf. on Rapidly Quenched Metals,* Elsevier Science Publishers, Netherlands, 1985, p. 1667.
10 P. Kasiraj, D. Kostka, T. Vreeland, Jr. and T. J. Ahrens, *J. Non-Cryst. Solids, 61/62* (1984) 967.
11 M. Sagawa, S. Fujimura, N. Togawa, H. Yamamoto and Y. Matsuura, *J. Appl. Phys., 55* (1984) 2083.
12 J. J. Croat, J. F. Herbst, R. W. Lee and F. E. Pinkerton, *J. Appl. Phys., 55* (1984) 2078.
13 K. H. J. Buschow, H. M. van Noort and D. B. de Mooij, *J. Less-Common Met., 109* (1985) 79.
14 T. Harada, T. Kuji, K. Fukuoka and Y. Syono, *J. Mater. Sci. Lett., 11* (1992) 1072.
15 Y. Syono and T. Goto, *AIP Conf. Proc., 78* (1982) 701.
16 J. Wecker and L. Schultz, *J. Appl. Phys., 62* (1987) 990.
17 T. Harada, T. Ando, R. C. O'Handley and N. J. Grant, *J. Appl. Phys., 68* (1990) 4728.
18 G. Schneider, E. T. Henig, G. Petzow and H. H. Stadelmaier, *Z. Metallkd., 77* (1986) 755.
19 G. Tu, Z. Altounian, D. H. Ryan and J. O. Ström-Olsen, *J. Appl. Phys., 63* (1988) 3330.
20 G. E. Carr, H. A. Davies and R. A. Buckley, *Mater. Sci. Eng., 99* (1988) 147.
21 G. Hilscher, R. Grössinger, S. Heisz, H. Sassik and G. Wiesinger, *J. Magn. Magn. Mater., 54–57* (1986) 577.
22 Y. Toda, T. Ogura, T. Masumoto, K. Fukuoka and Y. Syono, *Sci. Rep. Res. Inst. Tohoku Univ., Ser. A, 32* (1985) 267.
23 O. T. Inal, L. Keller and F. G. Yost, *J. Mater. Sci., 15* (1980) 1947.
24 J. D. Livingston, *J. Appl. Phys., 57* (1985) 4137.
25 R. J. Mishra, *J. Magn. Magn. Mater., 54–57* (1986) 450.
26 T. Harada, T. Ando, R. C. O'Handley and N. J. Grant, *J. Appl. Phys., 67* (1990) 4233.
27 A. Arora, D. B. Marshall, B. R. Lawn and M. V. Swain, *J. Non-Cryst. Solids, 31* (1979) 415.